



Papers

*Dedicated to the memory of
Academician Bogdan C. Simionescu (1948–2024)*

PHOTOCATALYTIC DEGRADATION OF ETHANOL DRIVEN BY PRISTINE AND METAL-MODIFIED TiO₂ OBTAINED BY SOL-GEL METHOD

Alexandra ILIE (SANDULESCU),^{a,*} Luminita PREDOANA,^a Crina ANASTASESCU,^a Jeanina PANDELE-CUSU,^a Silviu PREDA,^a Adriana RUSU,^a Daniela C. CULITA,^a Veronica BRATAN,^a Valentin Adrian MARALOIU,^b Valentin S. TEODORESCU,^{b,c} Ioan BALINT^a and Maria ZAHARESCU^a

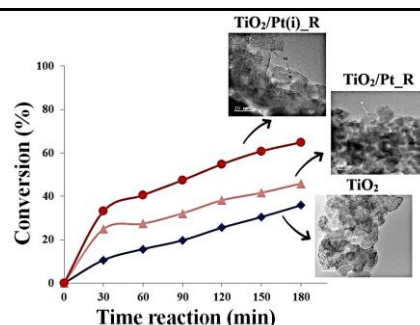
^a “Ilie Murgulescu” Institute of Physical Chemistry of the Roumanian Academy, 202 Spl. Independentei, 6th district, 060021 Bucharest, Roumania

^b National Institute of Materials Physics, 405 bis Atomistilor Street, 077125 Magurele-Ilfov, Roumania

^c Academy of Romanian Scientists, 3 Ilfov, 050044 Bucharest, Roumania

Received March 18, 2025

In the present paper the results regarding the preparation by sol-gel method of the pristine or Pt doped TiO₂ powders is presented. The doping was realized directly during the synthesis process (noted TiO₂/Pt_R) but also as surface modifiers of the pre-synthesized TiO₂ (noted TiO₂/Pt(i)_R). The aim of this research is to investigate the TiO₂ based sol-gel powders for the ethanol gas phase oxidative degradation assimilated to the indoor air purification. The structural, morphological and optical characterizations of the as obtained photoactive materials were analyzed in accordance with their functional properties described from the photocatalytic tests. The highest conversion of ethanol photodegradation (64.82%) was obtained in the case of TiO₂/Pt(i)_R powder after 3 hours of simulated solar light irradiation.



INTRODUCTION

Nanopowders with different compositions, purities, sizes, and dimensional distributions can be prepared using the sol-gel method. Two types of sol-gel processes are known based on the type of the precursors and on the reaction medium used: in alcoholic (organic) or in aqueous medium.^{1–3}

According to Pierre⁴ in both organic and aqueous sol-gel routes, the precursors undertake the succession of the following transformations in the presence of water:

Hydrolysis → Polymerization → Nucleation → Growth

Metal oxides, especially oxide semiconductor materials with large band gaps, have received much attention over the years due to their various electrical and optical properties. Titanium dioxide (TiO₂) has special applicability among broadband metal oxides. Its widespread use, particularly in photocatalytic processes, is owing to specific qualities such as excellent corrosion resistance and long life of excited electrons.⁵

* Corresponding author: asandulescu@icf.ro

Pristine and modified with noble metal titanium dioxide can be prepared using a variety of synthesis methods, both in the liquid phase (sol-gel method, hydrothermal method, microwave field synthesis, sonochemical method, or electrochemical synthesis) and in the vapor phase (pyrolysis, spraying, atomic layer deposition, chemical vapor phase deposition, or physical vapor phase deposition).^{6–10}

The sol-gel method is an effective and versatile method for generating TiO₂, and it can be used for both powder and film production.¹ Following the alkoxide route, the synthesis is carried out using alkoxides as titanium precursors, alcohol as solvent, water as reagent (in the hydrolysis reaction), and inorganic acids as catalysts. Thus, three-dimensional structures are formed that turn into gels, and these, through proper heat treatment, lead to amorphous or crystalline nanostructures (powders, films).¹¹

Titanium dioxide shows high photocatalytic activity, excellent functionality, high chemical and thermal stability, non-toxicity and low cost. It is known and used both as amorphous material and in crystalline forms (anatase, rutile and brookite). It has numerous applications – pigments, cosmetics, medicines, energy production, optical engineering, and nanobiotechnology. Platinum modified titanium dioxide is an advanced material used in various applications, especially in the field of catalysis and photocatalysis.^{8–10,12–14} Platinum acts as an “electron-sink” that reduces recombination of photogenerated charges, increasing the efficiency of photocatalytic processes.¹⁴ Doping can extend the sensitivity of TiO₂ to the visible region of the electromagnetic spectrum, which allows for efficient use of sunlight.¹⁵

The aim of this paper was to obtain by sol-gel method pristine TiO₂ powder but also modified with platinum, in order to test their photocatalytic

activity for the oxidative degradation of ethanol in the presence of simulated sunlight.

RESULTS AND DISCUSSION

Characterization of powders

The samples obtained in the conditions presented in the experimental part were white (pristine) or light grey powders for Pt modified TiO₂ and were investigated for their thermal behaviour, morphology, structure and photocatalytic properties.

The **FT-IR spectra** of TiO₂ and modified TiO₂ treated powders are shown in Fig. 1 and Table 1 presents the associated vibration bands. In the range of 3600–3200 cm⁻¹ the large band is noticed which corresponds to the structural OH groups and water vibrations and the vibration bands in the range of 3000–2900 cm⁻¹ correspond to C–H stretching vibrations in organic molecules, specifically from methyl groups. In the case of TiO₂ (Fig. 1a) spectrum a supplementary vibrations band around 2350 cm⁻¹ attributed to physical CO₂ gas absorbed at the surface of material is observed.

The band around 1600 cm⁻¹ is associated with the stretching vibration of physically adsorbed molecular water, while the bands between 1500–1300 cm⁻¹ corresponds to the vibration carbonates on the surface of samples. The bands between 1200–1000 cm⁻¹ corresponds to the C–O stretching vibration. The broad band between 600–500 cm⁻¹ is assigned due to νTi–O of condensed octahedral (TiO₆) with a small displacement to higher wavenumber values in case of doped samples (Figs. 1b and c).

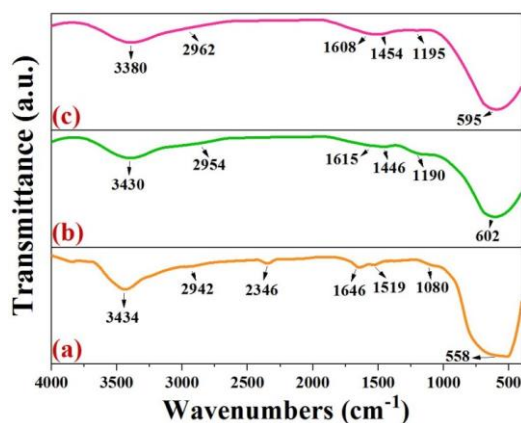


Fig. 1 – FT-IR spectra of the thermally treated samples: a) TiO₂; b) TiO₂/Pt_R; c) TiO₂/Pt(i)_R.

Table 1

Assignment of vibration bands in FT-IR spectra of samples

Wavenumbers (cm ⁻¹)			Assignments and vibration mode
TiO ₂	TiO ₂ /Pt_R	TiO ₂ /Pt(i)_R	
558	602	595	Ti-O stretching vibration of TiO ₆
1080	–	–	C–O
–	1190	1195	v _s (CO ₃) ²⁻
–	1446	1454	v _{as} (CO ₃) ²⁻
1519	–	–	δH ₂ O adsorbed water
1646	1615	1608	CO ₂ absorption
2346	–	–	C-H, v _{as} (CH ₃)
2942	2954	2962	vOH structural OH group
3434	3430	3380	

The small displacement to higher wavenumber values is assigned to the presence of dopants in the composition of the investigated samples.

The thermal behaviour of the as-prepared samples was examined using TG/DTG/DTA methods. Significant differences in thermal decomposition behaviour were not noticed regarding the as-prepared powders.

In Figure 2a, the titanium dioxide powder shows a total mass loss of 23.61% in the temperature range of 100–700°C that is due to the combustion of organic residues and the removal of structural hydroxyls. The sample shows two exothermic effects, one effect corresponding to the burning of organic residues is presented at 255°C, and the second attributed to crystallization, accompanied by dehydroxylation, is presented at 456°C.

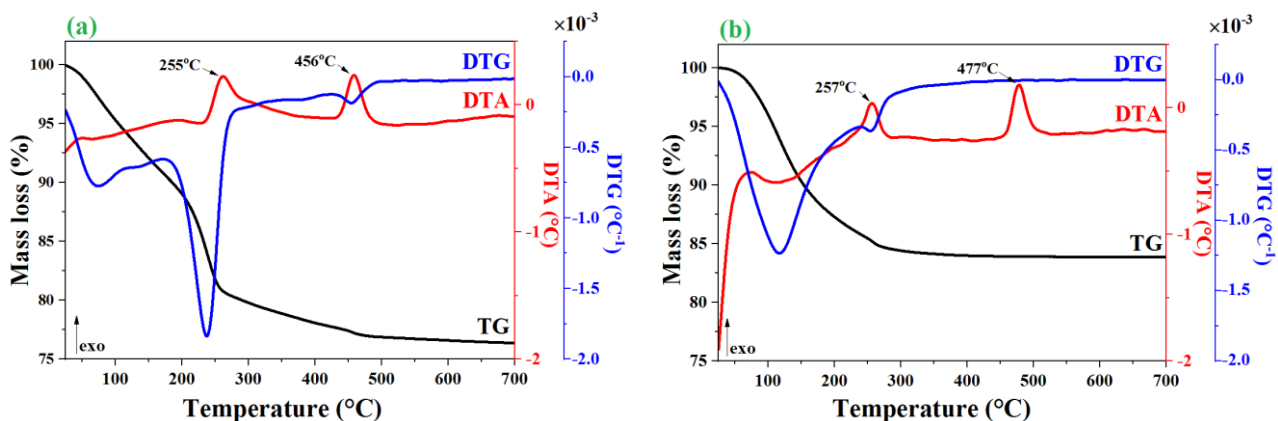


Fig. 2 – TG/DTG/DTA curves of the as-prepared samples: a) TiO₂; b) TiO₂/Pt_R.

In Figure 2b, the platinum-doped titanium dioxide (TiO₂/Pt_R) powder shows a total mass loss of 16.13%. As in the case of TiO₂ sample on DTA curves two exothermic effects occurs corresponding to the burning of the organic residues at 257°C, and that attributed to crystallization, at 477°C.

No weight loss is observed at temperatures higher than 500°C, for both analysed samples.

To obtain powders suitable for various applications, the as-prepared powders were thermally treated. The temperature of thermal treatment was determined based on TG/DTG/DTA results and was carried out at 500°C for 1 hour with a heating rate of 1°C/min.

The structural properties of the samples were examined using **Transmission electron microscopy** and the TEM micrographs were shown in Fig. 3. The TiO₂ sample (Fig. 3a), is formed by crystallites with dimensions of 20–60 nm, united in relatively welded aggregates. The surface of the anatase crystallites is irregular, they do not have shapes with surfaces formed by crystal planes (in the insert it is observed – in HRTEM – that the surface of the crystals is irregular).

In the case of TiO₂/Pt_R (Fig. 3b) a difference in sample morphology is observed. The surface of the anatase crystallites is smoother, but there are no majority crystalline planes, the surfaces being curved (insert – the

spherical particles of Pt on the surface of the anatase crystallites aggregates).

In the case of $\text{TiO}_2/\text{Pt}(i)_R$ (Fig. 3c), the 3.8 nm diameter Pt crystallite is at the edge of an anatase

crystallite. Pt nanocrystallites (even monocrystalline) are on the surface of the sample (insert – Pt nanoparticles are spherical and have dimensions from 2.5 nm to 6 or 7 nm. Most have sizes between 3 and 4 nm).

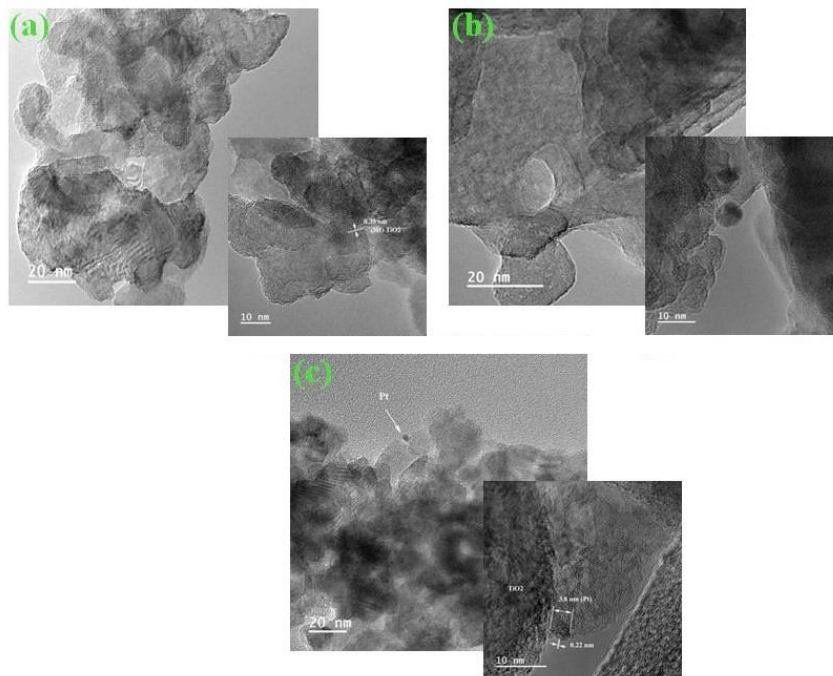


Fig. 3 – TEM micrographs of the nanopowders: a) TiO_2 ; b) TiO_2/Pt_R ; c) $\text{TiO}_2/\text{Pt}(i)_R$.

The **X-ray diffraction (XRD)** analysis was performed to determine the crystalline structure of the thermally treated samples, and the corresponding diffraction patterns are displayed in Fig. 4. The results indicate that all samples exhibit a single-phase anatase TiO_2 structure, as confirmed by the characteristic diffraction lines matching the reference pattern (ICDD #21-1272). No additional diffraction lines corresponding to other TiO_2

polymorphs, such as rutile or brookite, were observed. Furthermore, the absence of distinct lines associated with platinum-based compounds suggests that the incorporated Pt is either integrated into the anatase lattice in a substitutional or interstitial manner or remains in an amorphous state. This indicates that the introduction of Pt does not significantly alter the anatase phase composition, maintaining the structural integrity of TiO_2 .

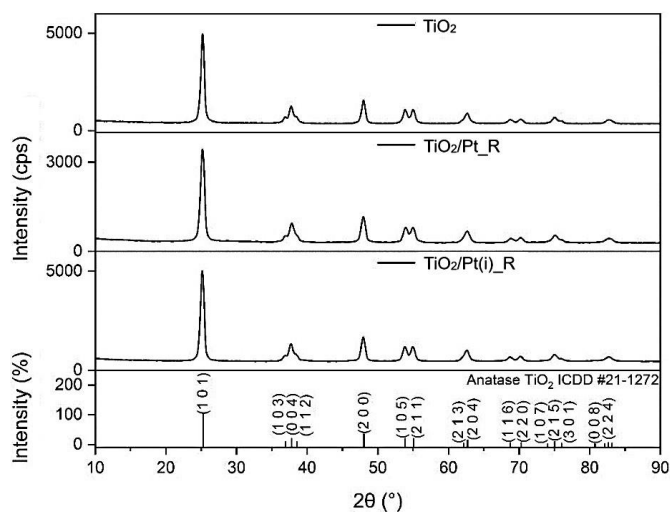


Fig. 4 – XRD patterns for powders thermally treated at 500°C 1h.

The lattice parameters and crystallite sizes of the anatase TiO₂ phase for the studied samples are presented in Table 2. The results indicate that all samples maintain a tetragonal anatase structure with minimal variations in lattice parameters. Notably, the Pt-impregnated sample (TiO₂/Pt(i)_R) exhibits a slightly larger lattice parameter along the c-axis (9.515 Å) and a marginally increased crystallite size (13.8 nm) compared to the pristine TiO₂ (9.506 Å, 12.9 nm) and the *in situ* Pt-doped

sample (TiO₂/Pt_R) (9.495 Å, 12.8 nm). These observations suggest that platinum incorporation may induce subtle structural modifications, potentially due to lattice distortion or the accommodation of Pt atoms within the anatase framework. However, the overall preservation of the anatase phase across all samples confirms that the thermal treatment at 500°C does not lead to significant phase transformations or polymorphic transitions.

Table 2

The lattice parameters and the crystallite sizes of the thermally treated samples

Sample	Crystalline phase	Lattice parameters (Å)			Crystallite size (nm)
		a	b	c	
TiO ₂	Anatase	3.786	3.786	9.506	12.9
TiO ₂ /Pt_R	Anatase	3.789	3.789	9.495	12.8
TiO ₂ /Pt(i)_R	Anatase	3.789	3.789	9.515	13.8

To evaluate the elemental composition of the studied samples and confirm the presence of the dopant element, **X-ray fluorescence (XRF)** analysis was conducted. The obtained results are summarized in Table 3. The analysis confirmed the presence of platinum (Pt) in the Pt-modified samples (TiO₂/Pt_R and TiO₂/Pt(i)_R) indicating successful incorporation of Pt into the material. The trace elements may originate from impurities in the precursor materials or minor contamination during sample preparation.

The platinum content in the Pt-modified samples

differs slightly, with TiO₂/Pt(i)_R containing a higher Pt mass percentage (1.05%) than TiO₂/Pt_R (0.51%), depending on the incorporation procedure. In case of impregnation method the higher amount of platinum can be explained by its presence on the surface of TiO₂ powder.

Overall, the XRF results confirm the successful integration of Pt into the TiO₂ matrix while maintaining the elemental integrity of the base material, with only negligible traces of extraneous elements present.

Table 3

Elemental composition of the analyzed samples

Sample	Composition	Values (Mass %)	Line
TiO ₂	Ti	59.25	Ti-KA
	O	39.57	O-KA
	Traces	1.18	
TiO ₂ /Pt_R	Ti	58.72	Ti-KA
	O	39.41	O-KA
	Pt	0.51	Pt-LA
	Traces	1.36	
TiO ₂ /Pt(i)_R	Ti	59.32	Ti-KA
	O	38.25	O-KA
	Pt	1.05	Pt-LA
	Traces	1.38	

For the **textural characterization** of the thermally treated powders, N₂ adsorption-desorption isotherms were recorded and are shown in Fig. 5. The textural parameters (BET surface area, micropore surface area, total pore volume, and average pore diameter) are listed in Table 4. All three samples exhibit type IV(a) isotherms with H3 hysteresis loops, as classified by IUPAC, which is characteristic of mesoporous materials

composed of non-rigid aggregates of plate-like particles with slit-shaped pores.¹⁶ The undoped TiO₂ and TiO₂/Pt_R samples have similar BET surface areas (~35 m²/g). However, *in situ* Pt doping leads to a reduction in micropore surface area from 11 m²/g to 3.2 m²/g compared to pure TiO₂. Simultaneously, a decrease in average pore diameter and total pore volume are observed. The sample modified by post-synthesis impregnation

(TiO₂/Pt(i)_R) exhibits a slightly larger BET surface area and total pore volume than pure TiO₂

but lacks micropores. Its average pore diameter is 11.8 nm, smaller than that of pure TiO₂.

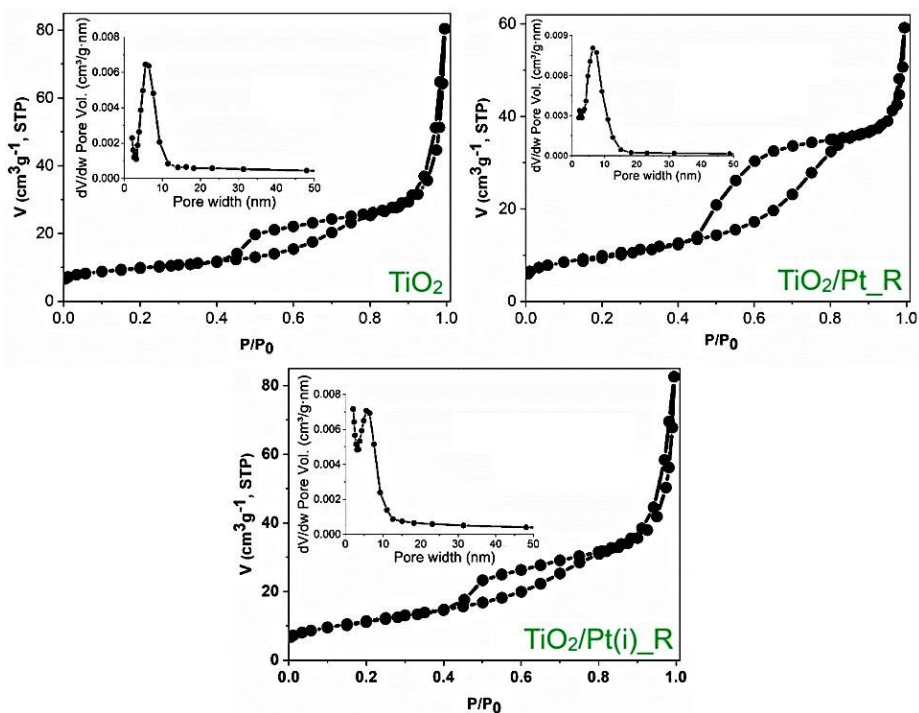


Fig. 5 – N₂ adsorption-desorption isotherms and pore size distributions (inset of the figures) of synthesized powders.

Table 4

The specific surface areas (S_{BET}), total pore volume (V_{total}) and average pore diameter (d_{BJH}) of the samples.

Sample	S_{BET} (m ² /g)	S_{micro} (m ² /g)	V_{total} (cm ³ /g)	d_{BJH} (nm)
TiO ₂	35.0	11.0	0.124	17.00
TiO ₂ /Pt_R	34.7	3.2	0.092	9.68
TiO ₂ /Pt(i)_R	40.8	0.0	0.128	11.80

UV-Vis absorption spectra of the thermally treated samples are illustrated in Fig. 6. All studied samples present a strong absorption in the UV region, with a sharp peak at ~340 nm, characteristic of TiO₂. This band is assigned to electronic transitions from O_{2p} to Ti_{3d}.¹⁷⁻¹⁸

Adding Pt increased the light absorption in the visible region. The band gap energies (E_g) were calculated considering indirect transitions and were listed in Table 5. It can be observed that their values were only slightly influenced by the Pt addition.

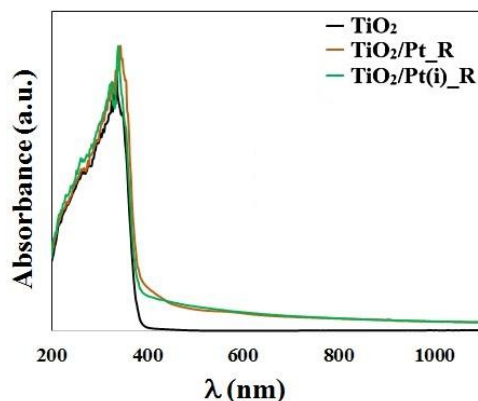


Fig. 6 – UV-Vis absorption spectra of synthesized powders.

Table 5

Optical bandgap of the thermally treated powders.

Sample	Bandgap
TiO ₂	3.1 eV
TiO ₂ /Pt_R	3.0 eV
TiO ₂ /Pt(i)_R	3.0 eV

Photocatalytic tests

Oxidative degradation in the presence of noble metal nanoparticles and metal nanoparticles supported by metal oxide is a common process, though in many cases, it does not result in the mineralization of pollutants.

Photocatalytic experiments were conducted in the gaseous phase, under temperature control, in air for three hours and under agitation to achieve equilibrium in the experimental system. Ethanol vapours are oxidized to intermediate products and finally to carbon dioxide and water under the action of solar simulated light in the presence of oxygen. The results have been corrected by extracting the blank test.

Table 6 shows the experimental results on the distribution of reactants and reaction products obtained from the oxidative degradation of ethanol in the gaseous phase under solar simulated light irradiation after 3 hours of reaction.

Table 6

Amount of measured compounds from oxidative degradation of ethanol in gaseous phase and ethanol conversion after 3 hours of reaction

Photocatalyst	C _{Inlet} (μmoles)	C _{Outlet} (μmoles)				Ethanol conversion (%)
	C ₂ H ₅ OH	C ₂ H ₅ OH	CH ₃ CHO	HCOOH	CO ₂	
TiO ₂	243.28	156.09	49.36	0.42	37.28	35.84
TiO ₂ /Pt_R	242.44	131.21	33.85	0.98	76.39	45.88
TiO ₂ /Pt(i)_R	243.06	85.49	44.93	1.97	109.66	64.82

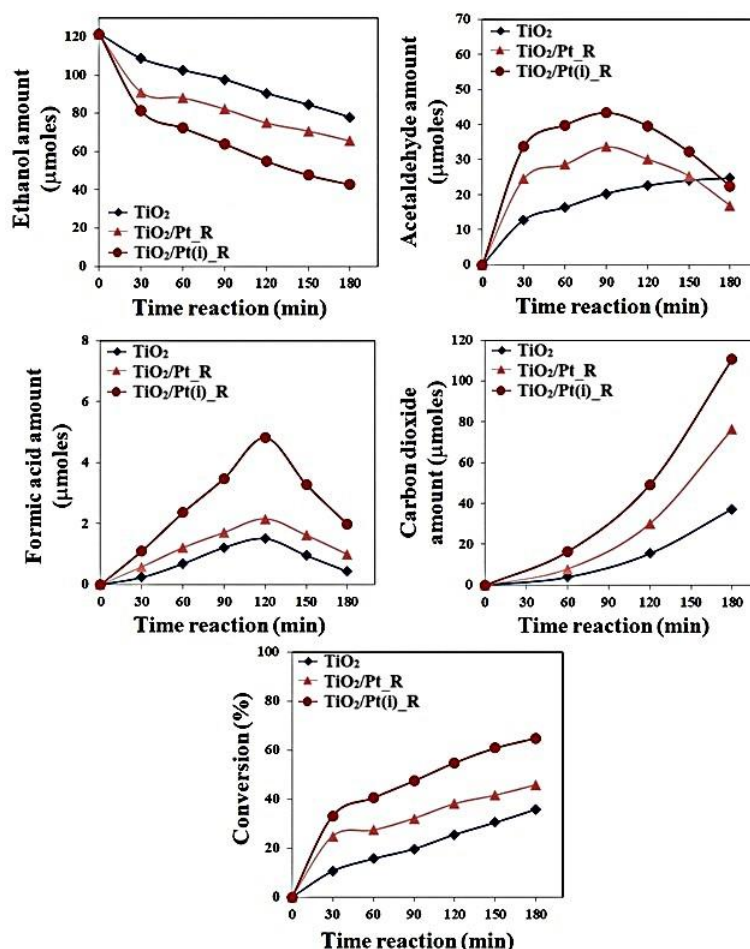


Fig. 7 – The results for the gaseous phase oxidative degradation of ethanol with pristine and Pt-doped TiO₂ catalysts exposed to simulated solar light.

At the end of the process, all catalysts produce mild ethanol oxidation products (CH₃CHO and HCOOH), as well as CO₂, with the best activity for TiO₂/Pt(i)_R catalyst. Platinum deposition increases catalytic activity during ethanol conversion (TiO₂ < TiO₂/Pt_R < TiO₂/Pt(i)_R).

Figure 7 presents the comparative results for the oxidative degradation of ethanol over all catalysts exposed to simulated solar radiation. CH₃CHO and HCOOH (minor) are produced sequentially in the mineralization process of C₂H₅OH at CO₂. The formation of acetaldehyde and formic acid occurs in the presence of both un-doped and platinum-doped TiO₂ powders. Highest photocatalytic activity was obtained in the case of the platinum-modified by post-synthesis impregnation powder (TiO₂/Pt(i)_R).

For TiO₂ powder the amount of acetaldehyde increases during the first 90 minutes of the reaction and then the reaction rate stabilizes, leading to the total oxidative conversion to carbon dioxide. In the case of powders doped with Pt, the amounts of acetaldehyde and tinny amount of formic acid is generated in the first half of the reaction, and then degrades significantly to carbon dioxide.

All three powders have a significant activity in the mineralization of ethanol in the gaseous phase, with the highest activity being the titanium dioxide modified with platinum by post-synthesis impregnation. An increase in the rate of CO₂ formation after the first hour of irradiation can also be observed, the mineralization of the generated intermediates being involved. The decreasing of the bandgap after Pt modification is in line with the improving of the photocatalytic activity of the samples TiO₂/Pt_R and TiO₂/Pt(i)_R. The fact that carbon dioxide is formed indicates a potential use for depollution since TiO₂ is a non-toxic and affordable material.

These results demonstrate the potential for practical utility of TiO₂ catalytic materials modified with Pt for the oxidative degradation of ethanol under solar simulated light.

Mechanism of oxidative degradation

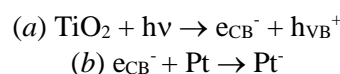
Oxidative photodegradation of organic compounds in the gaseous phase involves various processes. The first step in photocatalytic oxidation is the formation of electron-hole pairs.¹⁹⁻²⁰

The oxidative degradation of ethanol in the gaseous phase under solar-simulated light on TiO₂ and Pt-doped TiO₂ follows a photochemical

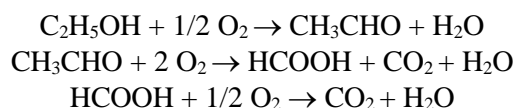
reaction mechanism involving molecular oxygen (O₂). The process leads to the formation of acetaldehyde (major product), formic acid, and carbon dioxide as the final oxidation product.²¹

Photoactivation of TiO₂ or Pt-TiO₂ – (a) under solar-simulated light, TiO₂ absorbs photons with energy equal to or greater than its bandgap (~3.2 eV for anatase). This excitation promotes an electron (e⁻) from the valence band (VB) to the conduction band (CB), generating an electron-hole pair (e⁻/h⁺); (b) Pt-doping enhances charge separation reducing recombination and increasing catalytic efficiency.²²⁻²³

The proposed mechanism is outlined below:



Overall Reactions



The ethanol photochemical degradation is increased with platinum adding, by reducing charge recombination. This occurs by oxidation of ethanol to acetaldehyde, formic acid and CO₂.

EXPERIMENTAL

Pristine or Pt-modified TiO₂ powders were prepared by the sol-gel method. The initial calculated compositions for doped powders prepared in situ synthesis correspond to a TiO₂:dopant oxide molar percentage of 99:1. The precursor for TiO₂ preparation was titanium (IV) isopropoxide [Ti[OCH(CH₃)₂]₄ (Merck) and for the Pt dopant was PtCl₄, isopropyl alcohol (i-C₃H₇-OH) (Merck) was used as solvent, H₂O as hydrolysis agent, and ammonium hydroxide [NH₄OH] (Riedel-de Haën) as catalyst. The molar ratio [Ti[OCH(CH₃)₂]₄:i-C₃H₇-OH:H₂O:NH₄OH = 1:5.4:6:0.3. The precursor's solution was homogenized at room temperature for 24 hours. The resulted powder was separated by filtration from the solution, washed with water to remove adsorbed reagents, dried at 80°C for 5 hours and then heat treated at 500°C, in air, with a plateau of 1 hour and a heating rate of 1°C/min in order to eliminate the water and organic residues and obtain crystallized nanometric powders.

In Figure 8 the preparation by the sol-gel method of the TiO₂ powder is presented.

The platinum was added by post-synthesis impregnation thus: in first order, the previously obtained nanopowder was dispersed in distilled water and then, an aqueous solution containing the dissolved 1 mol % PtCl_4 (platinum precursor) was slowly added to and left at room temperature, under continuous stirring, for 24 hours.

The process of metal reduction (in both cases of Pt-modified with platinum processes) was completed by adding of aqueous solution (5 mL) with dissolved NaBH_4 (0.04 g) to the TiO_2 suspension. The result materials was recovered by filtration and dried at 80°C for 5 hours.¹⁰

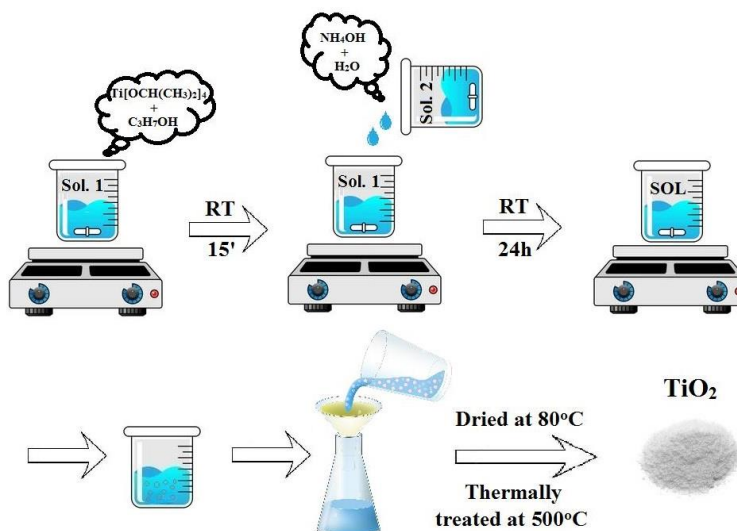


Fig. 8 – The flowchart of preparation of undoped and doped TiO_2 amorphous powders.

The samples were denoted TiO_2 , TiO_2/Pt_R (doped in situ) and $\text{TiO}_2/\text{Pt}(i)_R$ (modified by post-synthesis impregnation). The R noted represent the reduction process applied in case of both Pt-modified samples.

Methods of characterization

DTA/TG analysis was performed on Mettler Toledo 851^e equipment in Al_2O_3 crucibles with a heating rate of $10^\circ\text{C}/\text{min}$ in the gas flow (air) with a flow rate of $80\text{ mL}/\text{min}$.

Fourier-transform infrared spectra (FT-IR) were obtained using a Spectrometer Nicolet 6700 FT-IR (Thermo Electron Corporation) between 4000 and 400 cm^{-1} .

X-ray diffraction (XRD) of the powders were obtained using a Rigaku Ultima IV diffractometer, with $\text{Cu K}\alpha$ radiation (1.54056 \AA) with a scan rate of $1^\circ/\text{min}$ and 0.02°C step size, at 40 kV and 30 mA . The diffraction pattern ranging between 10° and 90° was recorded.

X-ray fluorescence (XRF) was performed using a Rigaku ZSX Primus II spectrometer (Rigaku Corp., Tokyo, Japan) equipped with a 4.0 kW X-ray Rh tube. Data processing was performed using EZscan combined with Rigaku SQX

fundamental parameters software, operating in a standardless mode.

Nitrogen adsorption-desorption isotherms at -196°C were recorded using a Micromeritics ASAP 2020 automated gas adsorption system (Norcross, GA, USA). The samples were degassed at 250°C for 4 h under vacuum before analysis. The specific surface area (S_{BET}) was calculated using the Brunauer-Emmett-Teller (BET) method. The microporosity contribution to the surface area (S_{micro}) of the materials was evaluated using the t-plot method, using the Harkins and Jura equation. Total pore volume was estimated from the amount adsorbed at relative pressure of 0.99 . The Barrett–Joyner–Halenda (BJH) method was applied to obtain the average pore diameter and pore size distribution curves using the adsorption data.

The **transmission electron microscopy (TEM)** observations were obtained using the JEOL ARM200F analytical electron microscope.

The **UV-Vis spectra** of the samples were recorded using a spectrophotometer Perkin Elmer Lambda 35, equipped with an integrating sphere. The measurements were carried out in the $1100\text{--}200\text{ nm}$ range, using spectralon as a reference. The reflectance measurements were converted to absorption spectra using the Kubelka-Munk function, $F(R)$. The optical bandgap was calculated using the

Tauc method. The linear region of the graphical representation of $[F(R)/h\nu]^{1/\eta}$ vs. $h\nu$ was extrapolated to 0 (where $h\nu$ is the energy of the photons and η is a parameter which has the value $1/2$ or 2 , for direct or indirect transitions, respectively). The intercept with the x-axis gets the band gap value.

The catalytic activity of the materials obtained was evaluated under solar-simulated light irradiation for the oxidative degradation of ethanol in the gaseous phase. The experiment involved dispersing 0.05 g of photocatalyst powder in a uniform layer with a surface area of approximately 3.6 cm² and a thickness of 1 mm. 7.2 μ L of ethanol was added to the photoreactor containing 120 cm³ of air, the experimental setup was left in the dark for half an hour. A cryostat was employed to control and keep temperature of the photoreactor at 25°C. The AM 1.5 (1000 W/m²) solar light was supplied by a Peccell L01 solar simulator. 200 μ L of gas samples were analyzed every 30 minutes using a gas chromatograph equipped with a Flame Ionization Detector (FID, Agilent 7890A), and 500 μ L of gas samples were analyzed every 60 minutes using a gas chromatograph equipped with a Thermal Conductivity Detector (TCD, Buck Scientific, model 90). The photocatalytic activity of the catalysts under investigation was observed for three hours.

CONCLUSIONS

In this paper, pure phase anatase and Pt-doped TiO₂ were synthesized by sol-gel method and tested as photocatalysts for oxidative degradation of ethanol in gaseous phase under solar simulated light. In the case of Pt-modified TiO₂, two methods of dopant introduction were used: (a) *in-situ* preparation and (b) the impregnation of the dopant post-synthesis of TiO₂ powder.

Both, support and noble metal catalyst, play an important role in light absorption, charge separation, and the formation of carbon dioxide which were analyzed for light-induced oxidation of ethanol on the noble metal (Pt) loaded with TiO₂. This study reveals the light-initiated photooxidative pathways for organic compounds over TiO₂ charged with a noble metal.

REFERENCES

1. S. Sakka, "Sol-gel process and applications", in "Handbook of Advances Ceramics", Amsterdam: Elsevier, 2013, pp. 883–910.
2. C. J. Brinker and G. W. Scherer, "Sol–Gel Science: The Physics and Chemistry of Sol–Gel Processing", San Diego: Academic Press, 1990, pp. 11–14.
3. K. Savolainen, H. Alenius, H. Norppa, L. Pylkkanen, T. Tuomi and G. Kasper, *Toxicology*, **2010**, 269, 92–104.
4. A. C. Pierre, "Sintering Sol-Gel Ceramics", in "Introduction to Sol-Gel Processing", Springer, 2020.
5. M. Pelaez, N. T. Nolan, S. C. Pillai, M. K. Seery, P. Falaras, A. G. Kontos, P. S. M. Dunlop, J. W. J. Hamilton, J. A. Byrne, K. O'Shea, M. H. Entezari and D. D. Dionysiou, *Appl. Catal. B: Environ.*, **2012**, 125, 331–349.
6. Y. Wang, Y. He, Q. Lai and M. Fan, *J. Environ. Sci.*, **2014**, 26, 2139–2177.
7. M. Malekshahi, A. N. Kharata, L. Fatholahib and Z. M. Beiranvand, *J. Nanostruct.*, **2013**, 3, 1–9.
8. E. Goncarenco, I. P. Morjan, C. T. Fleaca, F. Dumitrache, E. Dutu, M. Scarisoreanu, V. S. Teodorescu, A. Sandulescu, C. Anastasescu and I. Balint, *Beilstein J. Nanotechnol.*, **2023**, 14, 616–630.
9. E. Goncarenco, I. P. Morjan, E. Dutu, M. Scarisoreanu, C. Fleaca, L. Gavrilă-Florescu, F. Dumitrache, A. M. Banici, V. S. Teodorescu, C. Anastasescu, A. Sandulescu and I. Balint, *J. Solid State Chem.*, **2022**, 307, 122817.
10. A. Sandulescu, C. Anastasescu, F. Papa, M. Raculete, A. Vasile, T. Spataru, M. Scarisoreanu, C. Fleaca, C. N. Mihailescu, V. S. Teodorescu, N. Spataru, M. Zaharescu and I. Balint, *Catalysts*, **2021**, 11, 487.
11. C.M. Malengreaux, A. Timmermans, S.L. Pirard, S.D. Lambert, J.P. Pirard, D. Poelman and B. Heinrichs, Optimized deposition of TiO₂ thin films produced by a non-aqueous sol-gel method and quantification of their photocatalytic activity, *J. Chem. Eng.*, **2012**, 195–196, 347–358.
12. X. Chen and S. S. Mao, *Chem. Rev.*, **2007**, 107, 2891–2959.
13. C. Dong, J. Liu, M. Xing and J. Zhang, *Res. Chem. Intermediat.*, **2018**, 44, 7079–7091.
14. S. I. Shah, W. Li, C. P. Huang, O. Jung and C. Ni, *PNAS*, **2002**, 99, 6482–6486.
15. W. Fang, M. Xing and J. Zhang, *J. Photochem. Photobiol. C*, **2017**, 32, 21–39.
16. M. Thommes, K. Kaneko, A. V. Neimark, J. P. Olivier, F. Rodriguez-Reinoso, J. Rouquerol and K. S. W. Sing, *Pure Appl. Chem.*, **2015**, 87, 1051–1069.
17. B. Choudhury, M. Dey and A. Choudhury, *Nano Lett.*, **2013**, 3, 1–8.
18. A. Vasile, F. Papa, V. Bratan, C. Munteanu, M. Teodorescu, I. Atkinson, M. Anastasescu, D. Kawamoto, C. Negrila, C. D. Ene, T. Spataru and I. Balint, *J. Environ. Chem. Eng.*, **2022**, 10, 107129.
19. Y. Tulebekov, Z. Orazov, B. Satybaldiyev, D. D. Snow, R. Schneider and B. Uralbekov, *Molecules*, **2023**, 28, 6451.
20. Z. Shayegan, C. S. Lee and F. Haghghat, *J. Chem. Eng.*, **2018**, 334, 2408–2439.
21. K. Katsiev, G. Harrison, H. Alghamdi, Y. Alsalik, A. Wilson, G. Thornton and H. Idriss, *J. Phys. Chem. C*, **2017**, 121, 2940–2950.
22. Y. He, O. Dulub, H. Cheng, A. Selloni and U. Diebold, *Phys. Rev. Lett.*, **2009**, 102, 106105.
23. I. Sanusi and C. B. Almquist, *Catalysts*, **2023**, 13, 1203.